Acta Oncologica, 2014; 53: 1086–1092

informa
healthcare

ORIGINAL ARTICLE

Positron emission tomography and pharmacokinetics of 2-[18F]-fluoroethyl choline for metabolic studies in breast cancer xenografts

ALEXANDR KRISTIAN[1,2,3], PATRICK RISS[4,5], HONG QU[6], MONA MILDE[4], BENT W. SCHOULTZ[4], OLAV ENGEBRAATEN[1,2,3,7], GUNHILD M. MÆLANDSMO[1,3,8] & EIRIK MALINEN[9]

[1]*Department of Tumor Biology, Oslo University Hospital, Oslo, Norway,* [2]*Institute of Clinical Medicine, University of Oslo, Oslo, Norway,* [3]*K. G. Jebsen Center for Breast Cancer Research, University of Oslo, Oslo, Norway,* [4]*Department of Chemistry, University of Oslo, Oslo, Norway,* [5]*Norsk Medisinsk Syklotronsenter AS, Rikshospitalet, Oslo, Norway,* [6]*Institute for Basic Medical Sciences, University of Oslo, Oslo, Norway,* [7]*Department of Oncology, Oslo University Hospital, Oslo, Norway,* [8]*Department of Pharmacy, University of Tromsø, Tromsø, Norway and* [9]*Department of Physics, University of Oslo, Oslo, Norway*

ABSTRACT

Background. Breast carcinomas (BC) can have abnormal choline (Cho) metabolism. Earlier studies indicated that Cho uptake can differ between different subtypes of BC. The purpose of this study was to investigate uptake of 2-[18F]-fluoroethyl-choline ([18F]FECh) in three different patient-derived breast cancer xenografts (BCXs) using dynamic positron emission tomography (dPET).

Material and methods. Nine athymic nude mice bearing bilateral MAS98.12 (basal-like), HBCx34 or MAS98.06 (both luminal B) BCXs were subjected to a 90-minute dPET scan following a bolus injection of 10 MBq of [18F]FECh. A Patlak Plot analysis and a well-established two-tissue compartment model were fitted to the uptake curves of the whole tumors, providing estimates of transfer rates between the vascular, non-metabolized and metabolized compartments. Patlak slope K_P and intercept V, the rate constants k_1, k_2, k_3, the intravascular fraction vb and MR[18F]FECh were estimated. Additionally, analyses of terminal blood samples and tumor cell suspension incubated with [18F]FECh were performed.

Results. [18F]FECh uptake in all BCXs was similar to surrounding normal tissue, thus creating no image contrast. The average liver uptake was 10 times higher than the tumor uptake. The uptake in MAS98.12 was higher than in the other two BCXs during the whole course of the acquisition, and was significantly higher than in HBCx34 at 10–30 minutes after injection. No significant differences were found for k1, MR[18F]FECh and intravascular fraction vb. Patlak slope K_P, k_2 and k_3 were significantly lower for the MAS98.12 xenograft, in line with in vitro results. K_P was correlated with both MR[18F]FECh and k_3.

Conclusions. dPET demonstrated that different subtypes of breast cancer have different uptake of [18F]FECh. Differences in rate constants and K_P were in line with in vitro uptake in cell suspensions and earlier spectroscopy and gene expression analysis.

Tissue uptake of free choline (Cho) from the extracellular space, along with recycle of intracellular phosphocholine (PCho), are the sources of Cho for the de novo synthesis of phosphatidylcholine (PtdCho), a major phospholipid component of eukaryotic cells involved in building of a cellular membrane, signaling and lipoprotein metabolism [1]. Cho is taken through a membrane transporter and phosphorylated by choline kinase A (CHKA) or B (CHKB) to PCho. Further involvement of PCho in the metabolic pathway is dependent on the activity of enzymes and availability of diacylglycerols that, together with PCho, are precursors for PtdCho [1].

Correspondence: A. Kristian, Department of Tumor Biology, Division of Cancer Medicine, Surgery and Transplantation, Oslo University Hospital, Montebello, 0310 Oslo, Norway. E-mail: alexandr.kristian@gmail.com

(Received 14 May 2014; accepted 9 June 2014)

ISSN 0284-186X print/ISSN 1651-226X online
DOI: 10.3109/0284186X.2014.934398

Rapidly dividing cells, among them cancer cells, have elevated levels of Cho [2]. Studies performed in breast cancer cell lines and patient tumor biopsies have demonstrated elevated levels of Cho, PCho and glycerophosphocholine (GPCho), a product of PtdCho hydrolysis [3,4]. These levels of Cho metabolites may change as a result of treatment and a selective inhibition of Cho metabolism has been shown to have cytotoxic effect [5].

Several approaches may be useful to study Cho metabolism. Both ex vivo and in vivo magnetic resonance spectroscopy (MRS) [4,6,7] has been used to measure the concentration of Cho metabolites in normal and tumor tissue. Positron emission tomography (PET) with different Cho tracers so far has been used mainly for detection of cancer lesions [8]. We propose to use dynamic PET (dPET) with Cho tracers as a method to study the kinetics of the metabolism.

Several tracers have been used for imaging of tumors with high Cho uptake, among them [^{11}C]Cho [9] and 2-[18F]-fluoroethyl-choline ([^{18}F]FECh) [10]. In clinical practice Cho tracers are mainly used for detection of prostate cancer, including recurrent disease and metastasis, and some types of brain tumors [8]. [^{18}F]FECh is a preferable tracer due to easier logistics as a result of longer half-life with lower oxidation rate and comparable diagnostic value [11]. Several studies have focused on optimal timing for imaging of [^{18}F]FECh uptake both in prostate and brain tumors [12,13]. With the rapid decrease of [^{18}F]FECh concentration in the blood plasma, image acquisition as early as 5 minutes after tracer injection has been utilized. However, it has been demonstrated that delayed image acquisition can be favorable for differential diagnosis of brain tumors [12] and bone metastasis [8].

Few attempts have been made to establish a pharmacokinetic model for [^{18}F]FECh uptake and efforts have mainly been directed towards uptake in normal tissues [14,15]. To our knowledge there is only one study where a pharmacokinetic model has been applied for evaluating [^{18}F]FECh uptake in prostate cancer [16]. Earlier we have demonstrated that the rate constants from pharmacokinetic modeling of 18F-fluorodeoxyglucose uptake ([^{18}F]FDG) reflect glucose metabolism better than the standardized uptake value (SUV) [17]. Since the kinetics of [^{18}F]FECh uptake is similar to that of [^{18}F]FDG (including perfusion, membrane transport, a binding phase through phosphorylation, and finally trapping of the phosphorylated tracer inside the cell) we intended to examine whether two-tissue compartment pharmacokinetic model was also favorable in assessing Cho metabolism. In an animal study, Slaets and De Vos demonstrated that the Patlak plot analysis was a reliable and robust method for quantification of Cho metabolism [16]. In clinical practice time-resolved PET scans can be challenging. Thus the Patlak plot analysis of a semi dynamic acquisition at several time points could be used for assessment of irreversible tracer binding.

In this study we investigated whether [^{18}F]FECh dPET together with Patlak plot analysis and two-tissue compartment pharmacokinetic modeling of tracer uptake can be used to detect differences in Cho metabolism in patient-derived breast cancer xenografts (BCX).

Material and methods

Animals, xenografts and anesthesia

Three previously described patient-derived BCXs, one basal-like MAS98.12 [18] and two luminal-like MAS98.06 [18] and HBCx34 [19], inoculated in the mammary fat pads of female Athymic Nude-Foxn1^{nu} mice, were used in this study. Tumor inoculation, animal anesthesia and handling were performed as earlier described [20]. All experimental protocols were approved by The National Animal Research Authority and the experiments were conducted according to the regulations of the Federation of European Laboratory Animal Science Association (FELASA).

Dynamic PET measurements and 2-[18F]-fluoroethyl choline production

2-[18F]fluoroethyl choline was formulated as a clear, sterile solution in 0.9% NaCl with a pH between 5.5 and 7.5 with a radiochemical purity was $>$ 97%, as earlier described [21]. Dynamic [^{18}F]FECh PET was performed using a Siemens microPET Focus 120 (Erlangen, Germany) animal scanner. Animals were anesthetized, catheterized and handled before and during the acquisition as earlier described [20]. A 90 minute PET acquisition in list-mode was started prior to i.v. administration of 10 MBq [^{18}F]FECh) diluted in 0.9% NaCl solution. Three-dimensional (3D) dynamic emission data were reconstructed using OSEM3D-MAP (2 OSEM iterations, 18 MAP iterations, β 0.5, matrix size = $128 \times 128 \times 95$) [22], producing images with voxel size $0.87 \times 0.87 \times 0.87$ mm^3. The sampling time ranged from 10 seconds (early time points) to 600 seconds (late time points). All images were stored in microPET format and analyzed using PMOD software package (PMOD Technologies, Zurich, Switzerland).

Quantitative evaluation and kinetic modeling of dynamic [^{18}F]FECh PET

Pharmacokinetic analysis was performed using a full time two-tissue compartment kinetic model

(Supplementary Figure 1a, available online at http://informahealthcare.com/doi/abs/10.3109/0284186X.2014.934398) and a Patlak approach (Supplementary Figure 1b available online at http://informahealthcare.com/doi/abs/10.3109/0284186X.2014.934398) for acquisition times 20–90 minutes, both using individual Arterial Input Functions (AIFs). The AIF was obtained by linear interpolation between the measured values of the [^{18}F]FECh time activity curve (TAC) from the left ventricle and adjusted according to the amount of free [^{18}F]FECh. Tumors were manually delineated in the axial CT images and SUV TACs for individual tumors were obtained.

The median [^{18}F]FECh TAC for the whole tumor was subjected to kinetic modeling using a two-tissue compartment model (Supplementary Figure 1a available online at http://informahealthcare.com/doi/abs/10.3109/0284186X.2014.934398), described in detail elsewhere [23]. Briefly, the model assumes that the tracer concentration in the tissue, C_T, can be separated in a free (non-metabolized) and a bound (metabolized) compartment, with tracer concentrations C_F and C_B, respectively. The four rate constants in the model, k_1, k_2, k_3, and k_4, describes the exchange of [^{18}F]FECh between the blood pool and the two compartments. The kinetic parameters are estimated by non-linear least squares fitting of the model to the TAC. As phosphorylated [^{18}F]FECh was assumed to be trapped inside the cell, k_4 was set to zero. The metabolic rate of [^{18}F]FECh, $MR_{[18F]FECh}$, was calculated as $(k_1 \cdot k_3)/(k_2 + k_3)$. The goodness of fit between the measured TACs and the model fit was evaluated by Pearson's correlation coefficient squared (r^2). The Patlak plot analysis for irreversible binding was performed for acquisition times between 20 and 90 minutes (Supplementary Figure 1b available online at http://informahealthcare.com/doi/abs/10.3109/0284186X.2014.934398). The slope of the graph K_p and the intercept V, representing distribution volume, were calculated.

2-[18F]-fluoroethyl choline blood distribution

The free fraction of [^{18}F]FECh and its metabolites in the blood 90 minutes after the injection were determined as earlier described [24]. Briefly, 1 ml of blood was collected by heart puncture after the end of the dPET scan, 100IE of heparin (Leo, Ballerup, Denmark) was added immediately and the tube was placed on ice. Blood cell and protein fractions were separated by centrifugation and precipitation and the fractions activity was measured with a NaI(Tl) well counter (ORTEC Product Group, Oak Ridge, TN, USA). To detect [^{18}F]FECh metabolites, 0.2 ml plasma aliquots were deproteinated with 10% aqueous MeOH (400 µl), centrifuged at 5000 rpm for 5 minutes and the supernatant was analyzed by normal phase radio thin-layer chromatography.

In vitro 2-[18F]-fluoroethyl choline uptake

Tumor tissue from three different mice for MAS98.12 and MAS98.06 BCXs was mechanically disaggregated, washed three times in ice-cold PBS, and negatively filtered through a 70 µm filter. The pellet of 30 mg was resuspended in 3 ml of RPMI1640 tissue culture medium containing 5% serum, 2 mM L-alanine, 2 mM L-glutamine, and 20 mM HEPES. One MBq of [^{18}F]FECh in 0.2 ml 0.9% NaCl was added and the suspension was incubated in 90 minutes at 37°C. To analyze the bound and free [^{18}F]FECh, the suspension was incubated on ice for

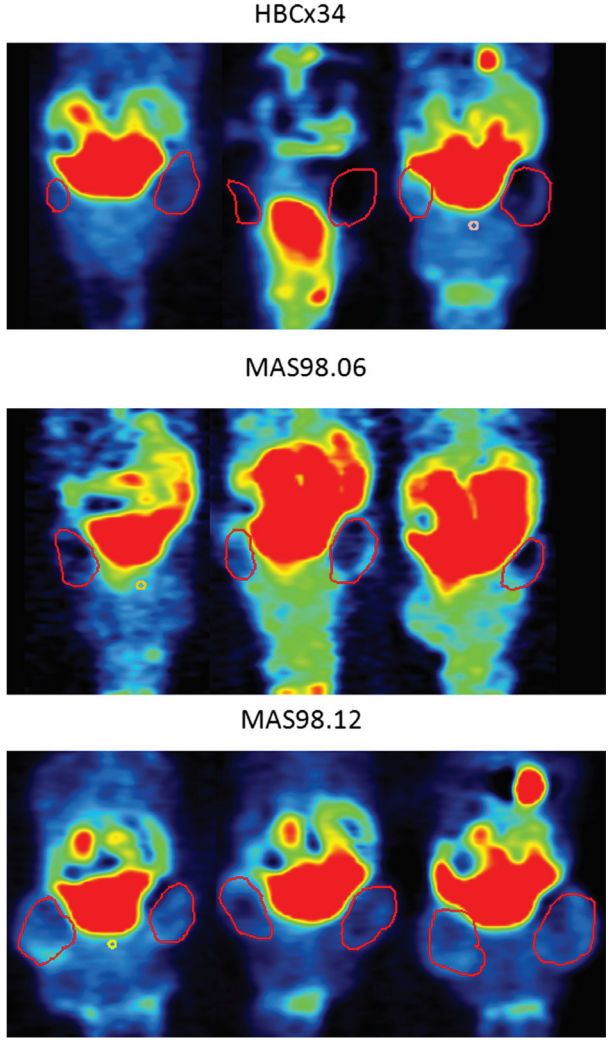

Figure 1. Coronal [^{18}F]FECh PET images for the HBCx34, MAS98.06 and MAS98.12 xenografts 90 minutes after [^{18}F]FECh injection. Red line indicates location of bilaterally implanted xenografts. Volumes of interest were delineated in the corresponding computer tomography image.

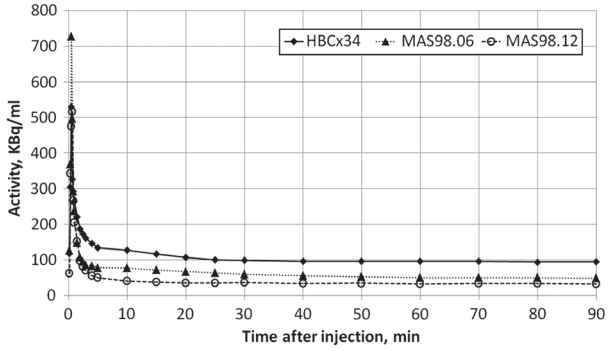

Figure 2. Mean arterial input functions for the HBCx34, MAS98.06 and MAS98.12 breast cancer xenografts.

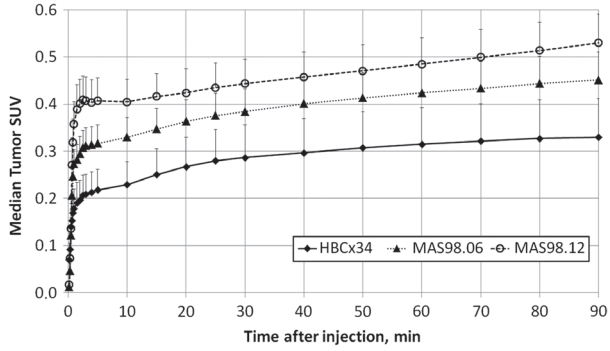

Figure 3. Median SUV curves for the HBCx34, MAS98.06 and MAS98.12 breast cancer xenografts at different time points after injection. Standard deviation for positive direction is shown.

30 minutes and then washed two times in ice-cold culture medium, centrifuged at 1000*g* to create a cell pellet and frozen in dry ice. The activity in the supernatants and the cell pellet was analyzed using a NaI well counter (ORTEC Product Group, Oak Ridge, TN, USA). The relative activity of the fraction was determined by dividing the count of the fraction at 511 keV by the count of the whole sample at 511 keV.

Statistics

For comparison of PET parameters in different BCXs, an ANOVA test with t-test as a post-hoc test was performed using SPSS 22. The statistical significance level chosen was 0.05. For correlation analysis Pearson's correlation coefficient was calculated.

Results

The [^{18}F]FECh tumor uptake 90 minutes post-injection was comparable to that in the surrounding normal tissue, and much lower than in the liver (Figure 1). Still, the uptake in the tumors was substantial, and further quantitative analysis was thus possible. All AIFs had a rapid decrease after initial bolus injection (Figure 2). The shape of the curves was similar for all animals. The tumor SUV rose quickly for the first 10 minutes, followed by a slower uptake phase (Figure 3). The SUV was less than 1 in all tumors for all time points. The uptake in MAS98.12 BCX was higher than in the other two BCXs during the whole course of the acquisition, and was significantly higher than in HBCx34 BCX at 10–30 minutes after injection. Also, only MAS98.12 BCX displayed a pronounced early uptake peak at roughly 2 minutes after injection. Average liver SUV was 10 times higher than in tumors.

Pharmacokinetic modeling data for both two-tissue compartment model and Patlak plot are presented in Table I. As reflected by the R^2 goodness of fit measure, the uptake curves could be fitted with comparably high accuracy for all three BCX. An example of fits to experimental data by the two-tissue compartment model for the three individual representative tumors for each BCX subtype is showed in Figure 4. Pearson's correlation coefficients between model parameters are presented in Table II. A strong correlation between k_3, $MR_{[18F]FECh}$ and K_P was found (Figure 5). After 90 minutes of incubation, uptake in MAS98.06 cell suspension was 4.2 times greater ($p = 0.035$) than in MAS98.12 cell suspension (Supplementary Figure 2, available online at http://informahealthcare.com/doi/abs/

Table I. Mean two-tissue compartment model and Patlak plot parameters and mean SUV for the HBCx34, MAS98.06 and MAS98.12 breast cancer xenografts.

	Two-tissue compartment model parameters						Patlak Plot parameters		SUV
Xenograft Name	Blood fraction, %	k_1, min^{-1}	k_2, min^{-1}	k_3, 10^{-3} min^{-1}	$MR_{[18F]FECh}$, 10^{-3}	R^2	K_P; 10^{-3} ml/min/ml	V	mean $SUV_{t=90}$
MAS98.12	0.9 (± 0.9)	0.06 (± 0.02)	0.11 (± 0.01)	9 (± 2)	4.3 (± 0.8)	0.97 (± 0.02)	3.3 (± 0.6)	0.56 (± 0.20)	0.53 (± 0.15)
HBCx34	2.0 (± 2.1)	0.06 (± 0.05)	0.21* (± 0.08)	9 (± 4)	3.2 (± 3.0)	0.97 (± 0.03)	2.5 (± 2.7)	0.35 (± 0.30)	0.33 (± 0.20)
MAS98.06	0.5 (± 0.3)	0.07 (± 0.01)	1.16* (± 0.01)	13* (± 2)	5.1 (± 0.3)	0.98 (± 0.01)	4.2* (± 0.3)	0.43 (± 0.04)	0.45 (± 0.12)

All values shown as mean ± SD. *$p < 0.05$, compared to MAS98.12 xenografts.

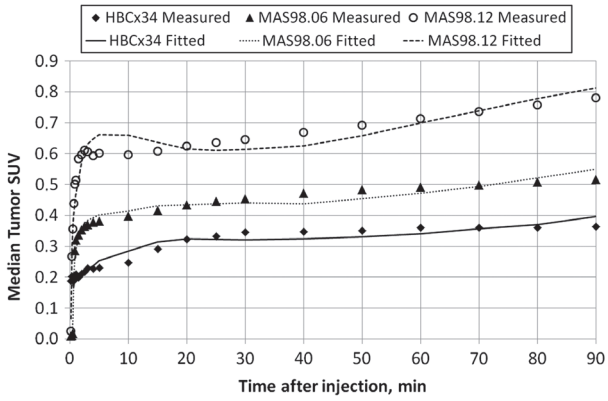

Figure 4. Measured SUV in the individual representative HBCx34, MAS98.06 and MAS98.12 breast cancer xenografts and corresponding fitted curves for a two-tissue compartment model.

10.3109/0284186X.2014.934398). For the terminal blood analysis, the blood cell fraction contained 68% of [^{18}F]FECh and its metabolites while 6% was bounded to plasma proteins and 26% was free. No [^{18}F]FECh metabolites were identified in the free plasma fraction.

Discussion

In this study we demonstrated the use of dPET for assessment of Cho metabolism in BCXs. The BCXs used were derived by implanting human tumor material in the mammary fat pads and have retained the morphology, gene expression pattern [18,19] and different Cho metabolic profiles found in the original patient tumor [3,4]. Pharmacokinetic rate constants reflected Cho metabolism, while both early (5 minutes after injection) and late (90 minutes after injection) time points SUV of [^{18}F]FECh failed to do so. Metabolic rate constant k3 was and $MR_{[18F]FECh}$ were correlated with Patlak slope K_P. In vitro uptake in cell suspension of BCX was in line with earlier gene expression and spectroscopy result [3].

Conventional PET imaging utilizes SUV derived from a single-frame acquisition. However, for evaluation of metabolic processes and discrimination of metabolic components a pharmacokinetic analysis can be helpful, especially when treatment effects following targeted therapy are being evaluated [20]. Optimal timing for [^{18}F]FECh have been investigated for different tumor types [8,12]. These studies showed that both early and late time points could be of value for detection of the tumor and differential diagnosis of the particular lesions. Unfortunately, early uptake is highly flow dependent, while late uptake is independent but creates less tissue contrast [13]. To overcome these problems we suggested to use [^{18}F]FECh dPET together with pharmacokinetic modeling or Patlak analysis.

For the two-tissue compartment model employed in the current study, three rate constants were used. The k_1 rate constant describes the transport of [^{18}F]FECh from plasma to the free intracellular compartment. The rate constant is dependent on the blood vessel perfusion and transporter abundance on the cellular membrane. MAS98.12 BCX was shown to have higher blood perfusion [17] and lower level of the Cho transporter SLC44A1[3] compared with MAS98.06 BCX. Although the results hinted towards higher initial uptake in MAS98.12 (Figure 1), we did not find any significant difference in k_1 rate constant for these two BCXs, suggesting that tumors with high perfusion and low abundance of the transporter will have the same influx of the tracer as tumors with low perfusion and high abundance of the transporter. The k_2 rate constant describes the efflux of the tracer. MAS98.12 had a significantly lower k_2 rate constant compared to MAS98.06. Combination of similar influx and higher efflux of the tracer resulted in lower SUV values for MAS98.06 BCX compared to MAS98.12 BCX.

The k_3 rate constant describes the transfer of tracer from the free to the bound intracellular compartment. In case of [^{18}F]FECh, it represents the activity of CHKA or CHKB [1]. MAS98.06 BCX has a higher expression of CHKA and CHKB genes compared to MAS98.12 BCX [3]. In our experiment MAS98.06 BCX demonstrated 1.45 times higher k_3 compared with MAS98.12 BCX, in line with gene expression analysis. In vitro uptake for MAS98.06 BCX was 4.2 times higher compared with MAS98.12. Taking into account absence of the perfusion component, higher level of a SLC44A1 transporter and

Table II. Pearson's correlation coefficients for two-tissue compartment model and Patlak plot parameters and mean SUV.

	SUV	Two-tissue compartment model parameters				
	mean $SUV_{t=90}$	Blood fraction	$MR_{[18F]FECh}$	k_1, min^{-1}	k_2, min^{-1}	k_3, min^{-1}
Patlak Slope, K_P	0.71†	−0.12	0.97†	0.48	−0.58*	0.57*
Intercept, V	0.81†	0.44	0.80†	0.80†	−0.39	0.04
SUV mean, 90 minutes post-injection		0.11	0.87†	0.52*	−0.50	0.31
Blood fraction			0.08	0.71†	0.46	−0.36
$MR_{[18F]FECh}$				0.69†	−0.50	0.59*

*$p < 0.05$; †$p < 0.01$.

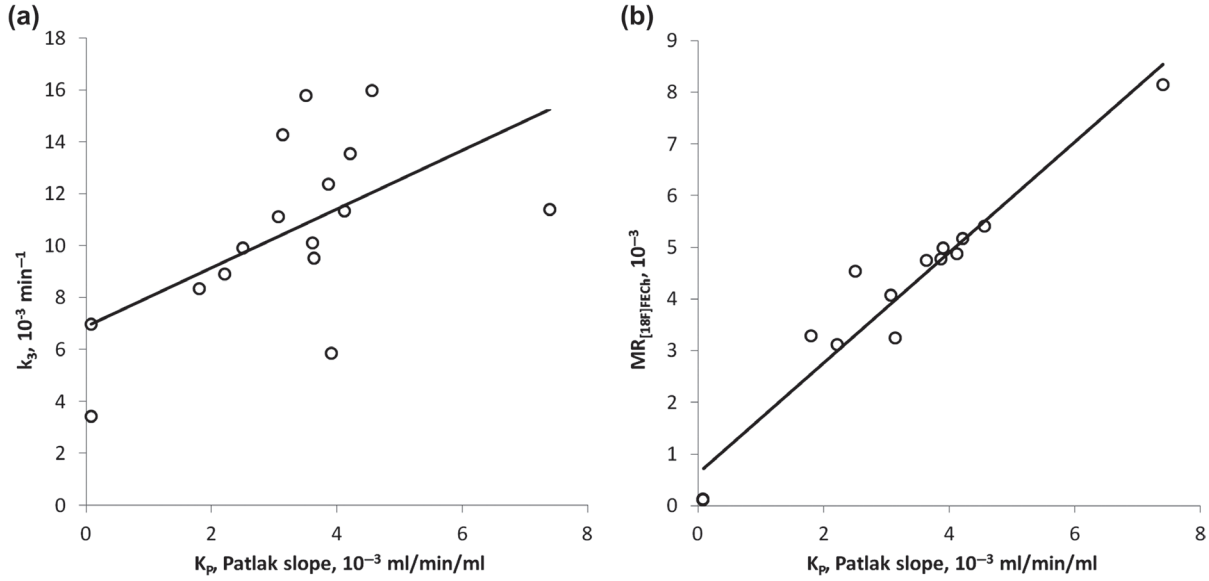

Figure 5. (a) Relationship between Patlak slope KP and metabolic rate constant k_3. Regression line: y = 1.13x + 0.01, r = 0.57. (b) Relationship between Patlak slope K_P and metabolic rate $MR_{[18F]FECh}$. Regression line: y = 0.87x–0.001, r = 0.97.

CHKA and CHKB kinases resulted in a significantly higher levels of [^{18}F]FECh in MAS98.06 BCX compared to MAS98.12 BCX.

A Patlak plot analysis for time points between 20 and 90 minutes was performed. A Patlak slope K_P that should estimate irreversible binding rate of the tracer and should be flow independent was higher for MAS98.06 BCX and correlated with the k_3 rate constant. K_P was also strongly correlated with $MR_{[18F]FECh}$. This is in line with the assumption of the irreversible binding of [^{18}F]FECh in the cell.

Both models used in this study strongly rely on the correct estimation of AIF. We observed rapid clearance of [^{18}F]FECh from plasma. Only 26% of the tracer was free in the terminal blood sample, in line with previous reports [16]. The rapid clearance of [^{18}F]FECh led to a low residual blood activity at late time point and count rates were generally in the low counts per minute range. Two-tissue pharmacokinetic model employ three rate constants and do not account for rapid clearance from the blood due to binding of the tracer to the blood component. While for poor vascularized HBCx34 and MAS98.06 no significant alteration were noticed and the model fit was satisfactory, for some tumor of MAS98.12 well vascularized BCX the fit differed from the measure data. However, this model fail did not affect the estimation of k_3 rate constant.

Although no major metabolites were identified in the samples, these results may be somewhat confounded by a poor signal to noise ratio. This finding is in line with earlier studies that demonstrated lower oxidation of [^{18}F]FECh [16] compared to [^{11}C]Cho. A study by Slaets and De Vos [16] suggested an additional metabolized compartment for [^{18}F]Betaine, a product of [^{18}F]FECh oxidation, in the pharmacokinetic modeling. However, the non-linear fitting to the experimental data was not improved by including this compartment in the model in line with Slaets and De Vos report. In our experiments the fitting quality was good and with R^2 above 0.9 for all tumors without exception. Our experience suggests that introduction of several compartments or rate constants in the models do not improve the fitting, but may rather complicate and mislead the interpretation of the results.

SUV was higher, although non-significant, for MAS98.12 for all time points compared to MAS98.06. SUV, especially for early time points, is highly perfusion dependent. As a result a conventional [^{18}F]FECh PET that is taken 5 minutes after tracer injection is measuring tumor perfusion and transporter density rather than Cho metabolism [13]. Therefore, one should be careful when interpreting the effect of treatment on Cho metabolism based on [^{18}F]FECh PET uptake at early time points.

In conclusion, we have demonstrated that [^{18}F]FECh can be used as a dPET tracer for assessment of choline metabolism in patient-derived BCX. [^{18}F]FECh is not subjected to oxidation in the same manner as [^{11}C]Cho and a simple two-tissue compartment pharmacokinetic model can be used to describe the uptake. The process of Cho metabolism is dynamic and is balanced by influx and efflux of Cho in the cells [1]. Both spectroscopy and gene expression analysis gives a snapshot of it, rather than depicting the dynamics. [^{18}F]FECh PET at early time points can be misleading when used for evaluation of Cho metabolism due to strong perfusion effects. Pharmacokinetic rate constants

should be preferable for evaluation of Cho metabolism. However, for clinical use, when fully time-resolved dynamic imaging is not possible, a Patlak plot analysis can be used as well.

Acknowledgements

Financial support received from the K.G. Jebsen Center for Breast Cancer Research is gratefully acknowledged.

Declaration of interest: The authors report no conflicts of interest. The authors alone are responsible for the content and writing of the paper.

References

[1] Podo F. Tumour phospholipid metabolism. NMR Biomed 1999;12:413–39.
[2] Eliyahu G, Kreizman T, Degani H. Phosphocholine as a biomarker of breast cancer: Molecular and biochemical studies. Int J Cancer 2007;120:1721–30.
[3] Moestue SA, Borgan E, Huuse EM, Lindholm EM, Sitter B, Borresen-Dale AL, et al. Distinct choline metabolic profiles are associated with differences in gene expression for basal-like and luminal-like breast cancer xenograft models. BMC Cancer 2010;10:433.
[4] Grinde MT, Skrbo N, Moestue SA, Rodland EA, Borgan E, Kristian A, et al. Interplay of choline metabolites and genes in patient-derived breast cancer xenografts. Breast Cancer Res 2014;16:R5.
[5] Banez-Coronel M, Ramirez de Molina A, Rodriguez-Gonzalez A, Sarmentero J, Ramos MA, Garcia-Cabezas MA, et al. Choline kinase alpha depletion selectively kills tumoral cells. Curr Cancer Drug Targets 2008;8:709–19.
[6] Esmaeili M, Moestue SA, Hamans BC, Veltien A, Kristian A, Engebraten O, et al. In Vivo 31 P magnetic resonance spectroscopic imaging (MRSI) for metabolic profiling of human breast cancer xenografts. J Magn Reson Imaging Epub 2014 Feb 14.
[7] Tozaki M. Proton MR spectroscopy of the breast. Breast Cancer 2008;15:218–23.
[8] Rice SL, Roney CA, Daumar P, Lewis JS. The next generation of positron emission tomography radiopharmaceuticals in oncology. Semin Nucl Med 2011;41:265–82.
[9] Hara T, Kosaka N, Kishi H. PET imaging of prostate cancer using carbon-11-choline. J Nucl Med 1998;39:990–5.
[10] DeGrado TR, Reiman RE, Price DT, Wang S, Coleman RE. Pharmacokinetics and radiation dosimetry of 18F-fluorocholine. J Nucl Med 2002;43:92–6.
[11] Brogsitter C, Zophel K, Kotzerke J. 18F-Choline, 11C-choline and 11C-acetate PET/CT: Comparative analysis for imaging prostate cancer patients. Eur J Nucl Med Mol Imaging 2013;40:18–27.
[12] Mertens K, Bolcaen J, Ham H, Deblaere K, Van den Broecke C, Boterberg T, et al. The optimal timing for imaging brain tumours and other brain lesions with 18F-labelled fluoromethylcholine: A dynamic positron emission tomography study. Nucl Med Comm 2012;33:954–9.
[13] Price DT, Coleman RE, Liao RP, Robertson CN, Polascik TJ, DeGrado TR. Comparison of [18 F]fluorocholine and [18 F]fluorodeoxyglucose for positron emission tomography of androgen dependent and androgen independent prostate cancer. J Urol 2002;168:273–80.
[14] Tavola F, Janzen T, Giussani A, Facchinetti D, Veronese I, Uusijarvi-Lizana H, et al. Nonlinear compartmental model of 18F-choline. Nucl Med Biol 2012;39:261–8.
[15] Giussani A, Janzen T, Uusijarvi-Lizana H, Tavola F, Zankl M, Sydoff M, et al. A compartmental model for biokinetics and dosimetry of 18F-choline in prostate cancer patients. J Nucl Med 2012;53:985–93.
[16] Slaets D, De Vos F. Comparison between kinetic modelling and graphical analysis for the quantification of [18F]fluoromethylcholine uptake in mice. EJNMMI Res 2013;3:66.
[17] Kristian A, Nilsen L, Røe K, Revheim M-E, Engebråten O, Mælandsmo G, et al. Dynamic 18 F-FDG PET for assessment of tumor physiology in two breast carcinoma xenografts. Nucl Med Mol Imaging 2013;47:173–80.
[18] Bergamaschi A, Hjortland GO, Triulzi T, Sørlie T, Johnsen H, Ree AH, et al. Molecular profiling and characterization of luminal-like and basal-like in vivo breast cancer xenograft models. Mol Oncol 2009;3:469–82.
[19] Marangoni E, Vincent-Salomon A, Auger N, Degeorges A, Assayag F, de Cremoux P, et al. A new model of patient tumor-derived breast cancer xenografts for preclinical assays. Clin Cancer Res 2007;13:3989–98.
[20] Kristian A, Revheim ME, Qu H, Maelandsmo GM, Engebraten O, Seierstad T, et al. Dynamic (18)F-FDG-PET for monitoring treatment effect following anti-angiogenic therapy in triple-negative breast cancer xenografts. Acta Oncol 2013;57:1566–72.
[21] Riss PJ, Hoehnemann S, Piel M, Roesch F. Two-step radiosynthesis of 18)F]FE-beta-CIT and [18F]PR04.MZ. J Labelled Comp Radiopharm 2013;56:356–9.
[22] Qi J, Leahy RM. Resolution and noise properties of MAP reconstruction for fully 3-D PET. Med Imaging 2000; 19:493–506.
[23] Roe K, Aleksandersen TB, Kristian A, Nilsen LB, Seierstad T, Qu H, et al. Preclinical dynamic 18F-FDG PET – tumor characterization and radiotherapy response assessment by kinetic compartment analysis. Acta Oncol 2010; 49:914–21.
[24] Riss PJ, Hong YT, Williamson D, Caprioli D, Sitnikov S, Ferrari V, et al. Validation and quantification of [18F]altanserin binding in the rat brain using blood input and reference tissue modeling. J Cereb Blood Flow Metab 2011;31:2334–42.

Supplementary material available online

Supplementary Figures 1–2 and Appendix available online at http://informahealthcare.com/doi/abs/10.3109/0284186X.2014.934398.